Vector-spherical-harmonics representation of vector complex source beams carrying vortices

S. Orlov ●[*] and J. Berškys

Center for Physical Sciences and Technology, Coherent Optics Laboratory, Sauletekio ave 3, LT-10257 Vilnius, Lithuania

Vectorial solutions of Maxwell's equations describing highly focused and variously polarized vector complex source vortex beams are investigated. An analytical representation of these beams in the vector-spherical basis of electromagnetic multipoles is presented. In particular, three different families of optical vector vortex beams are studied in detail. Whereas the vortical solutions derived within spherical symmetry can be represented only by electric (magnetic) multipoles, solutions derived within cylindrical and Cartesian symmetry also exhibit magnetic (electric) multipole components. We utilize the representation of the studied beams in vector-spherical harmonics to investigate their interaction with a cluster of nanoparticles.

I. INTRODUCTION

Nanoparticles are at the focus of active research in nanosciences. The first description of light interaction with a particle started with Mie theory [1]. In contrast to plane-wave illumination, the rising interest in highly focused vectorial light beams is mainly concerned with their polarization distribution, which strongly influences the size and shape of the focal spot of the beam [2,3]. Recent publications [4–7] investigate interaction between these beams and structures having subwavelength dimensions. The knowledge of interaction results can be applied for a nanointerferometric beam reconstruction of radially and azimuthally polarized beams [8], and was even demonstrated on reconstruction of Mobius strips [9] and multitwist ribbons [10] polarization distribution beams. These works have clearly demonstrated that the optical response is strongly dependent on both the particle location relative to the beam in the focus and the polarization state of the beam. Results show noticeable difference from the results retrieved solely from classical Mie theory.

To tackle this problem, the theoretical description of the tightly focused beams is needed. One can start from exact analytical solutions of the scalar Helmholtz equation $\Delta u(\mathbf{r}) + k^2 u(\mathbf{r}) = 0$ (see Refs. [11,12]) using the monochromatic complex source beam (CSB) model, described by the solution of the equation $u(\mathbf{r})$ [13,14] and extend it towards full vectorial solutions of Maxwell's equations [15–18]. This approach can be adapted to construct highly focused vectorial beams within spherical, cylindrical, and Cartesian symmetries from scalar complex source vortices [19], which are a good approximation [16] both for experimentally realizable beams and their numerical approximations that use integrals of Richards and Wolf [20]. We note that optical vortices derived within Cartesian symmetry exhibit properties analogous to circularly and linearly polarized highly focused vortex beams. Vortical CSB

solutions derived within cylindrical and spherical symmetry have intriguing properties [19].

Optical vortices are spiral phase ramps $\exp(im\phi)$ around a point, where the phase of the beam is undetermined (singular) and its amplitude vanishes as $\rho^{|m|}$ [21,22]. Here, (ρ, ϕ) are polar coordinates. The order $l = |m|$ of the phase singularity (also of the root of the radial dependence of the basis functions) multiplied by its sign α is referred to as the topological charge m of the vortex. Phase singularities (vortices) can be generated experimentally by a variety of different techniques utilizing, for instance, a spiral plate [23], mode converters [24], phase masks [25], or an axicon [26]. Optical vortices are widely known for their applications in optical tweezers [27] and optical spanners [28], which enable the manipulation of nanoparticles [29], biological cells [30], or bacteria [31]. An addition of a small coherent background splits an initially multiple charged vortex into $|m|$ single-charged vortices [32]. It was demonstrated that in the near field the superposition of two coaxial Bessel-Gauss (BG) singular beams creates a light pattern with complicated vortical structures which due to diffraction dynamically evolves into rather simple structures [33,34].

Complexified optical vortices are very common in photonics and can be found in many of its branches. For example, as Siegman [11] noticed, Laguerre-Gaussian modes are complexly displaced. The dependence of field distribution on propagation distance z has a form $z \pm iz_0$, where z_0 is the Rayleigh (diffraction) length $z_0 = kw_0^2/2$ of Laguerre-Gaussian beams [11] and k is the wave vector with w_0 being the beam width.

To simplify the analysis of interaction between the light field and nano-object, an introduction of vector-spherical harmonics (VSH), electromagnetic multipoles [12], is required. When both an object and an incoming beam are properly described using VSHs, the interaction of nano-object with the light is theoretically solvable [35–37], therefore, it is preferable to decompose incoming light field into multipoles to ease the analysis and reduce complexity. Moreover, the multipole approach also provides an efficient method for calculating the

---

*Sergejus.Orlovas@ftmc.lt

field in the focal region of a lens [38] and allows tailoring of multipolar Mie scattering with helicity and angular momentum [39]. It was also shown that the the interaction of a beam with larger objects, which are conveniently described by a T matrix [40], can be readily described with the multipole decomposition of the incident beam. This approach has enabled simulation of nonspherically shaped particles [6] or various clusters of them [41,42]. Most importantly, a flexible control of the multipoles in the incident beam has enabled selective excitation of single resonances in particles [36]. Therefore, for the description of the interaction between an object and a highly focused structured light, a knowledge of expansion coefficients is required.

The underlying spherical symmetry of the complex source beams, which are obtained by a complex displacement in respect to their propagation axis [13,43], ensures that they can be easily expanded into nondisplaced scalar multipoles [44] or can be used as basis functions [45]. This allows analytical expansion of highly focused radially, azimuthally, and linearly polarized beams into vector-spherical harmonics (VSH), therefore, analytical study of their interaction with a polarizer is possible [46]. Those analytical results have enabled a better understanding of transverse spin in the scattering of focused radially and azimuthally polarized vector beams [47]. Moreover, the complex displacement of the coordinates [48] in the VSHs results in an interesting set of eigenfunctions [49,50], that enables analysis of Fano resonances in photonic molecules [51] and generation of an optical ball bearing facilitated by coupling between handedness of polarization of light and helicity of its phase [52].

In this paper we will follow the investigation path described earlier for scattering analysis of novel vector vortex beams, which were introduced recently in a CSB description [19], by three spherical nanometer-sized spheres. We will analytically decompose the three different families of focused vector beams in the vector-spherical basis and show scattered electromagnetic field by subwavelength dimension spheres.

II. EXPANSION OF HIGHLY FOCUSED VECTOR VORTEX BEAMS INTO VSH

A. Expansion of scalar complex source vortex beams

Scalar CSB solutions are defined as [13]

$$\begin{Bmatrix} \mathrm{Rg}\, u(\mathbf{r}) \\ u(\mathbf{r}) \end{Bmatrix} = \begin{Bmatrix} j_\nu(ks) \\ h_\nu^{(1)}(ks) \end{Bmatrix} P_\nu^\mu(\cos\Theta) \exp(i\mu\phi), \quad (1)$$

with j_ν and h_ν being spherical Bessel functions of the first and third kind, P_ν^μ is the associated Legendre polynomial, which we define as in [40], and ν, μ are integer numbers, and the complex angle Θ is defined by $s(\mathbf{r})\sin\Theta = (x^2 + y^2)^{1/2}$. Here, the first line corresponds to the regular solution (suffix "Rg") and the second line to the irregular one. The complex distance s is defined as $s(\mathbf{r}) = [x^2 + y^2 + (z - iz_0)^2]^{1/2}$ in Cartesian or as $s(\mathbf{r}) = [r^2 - 2irz_0\cos\theta - z_0^2]^{1/2}$ in spherical coordinates [$\mathbf{r} = (r, \theta, \phi)$], where $z_0 = kw_0^2/2$ is the Rayleigh length and w_0 is the beam width [11]. We note that the complex distance $s(\mathbf{r})$ leads to the appearance of the Gouy phase and physically introduces beam to the diffraction via its dependance on diffraction length z_0 [11]. To guarantee

a constant power flow in the forward direction we make the "beam" choice with a branch cut ($\mathrm{Im}[s(\mathbf{r})] \leqslant 0$) [13,16], where the irregular solution also includes a ring of sources at $x^2 + y^2 = z_0^2$ (for a more detailed discussion of the different solutions, see [16]). We remind here that m is the topological charge of the Laguerre-Gaussian (LG) vortex, $l = |m|$ is the magnitude, and $\alpha = \pm 1$ is the sign of the topological charge (or the sign of the phase singularity [22]). The CSB solution (1) represents a LG vortex only in one particular case, when $\mu = m$ and $\nu = l$ (see Ref. [19]). For positive m we can use $P_m^m = (-1)^m (2m - 1)!!\sin^m\Theta$ in Eq. (1) and obtain

$$\begin{Bmatrix} \mathrm{Rg}\, u(\mathbf{r}) \\ u(\mathbf{r}) \end{Bmatrix} = U_0 \begin{Bmatrix} j_l(ks) \\ h_l^{(1)}(ks) \end{Bmatrix} \left(\frac{R\sin\theta}{s}\right)^l e^{i\alpha l\phi}$$

$$= U_0 g_l(ks)\left(\frac{R\sin\theta}{s}\right)^l e^{im\phi}, \quad (2)$$

which is an expression for a scalar complex source vortex (CSV). Here, g_l is either a regular (nonsingular) spherical Bessel function of the first kind j_l, or an irregular (singular) function of the third kind $h_l^{(1)}$. The normalization constant U_0 ensures that the on-axis value of the beam is unity for $l = 0$ and also makes on-axis expressions easier to handle. Mostly important, due to the normalization constant U_0 the electric field is measured from now on in dimensionless units. We define it as

$$U_0 = \frac{(-ikz_0)^l}{g_l(-ikz_0)}. \quad (3)$$

The expression for negative m can be obtained via $P_l^{-m} = (-1)^m (l - m)!/(l + m)! P_l^m$.

We start with the expansion of the scalar CSV (1) into scalar multipoles [12], which are the eigenfunctions of the scalar wave equation in spherical coordinates and can be obtained from Eq. (1) by setting the complex displacement $z_0 = 0$:

$$u_{\mu\nu}(\mathbf{r}) = g_\nu(kr)P_\nu^\mu(\cos\theta)\exp(i\mu\phi). \quad (4)$$

The expansion is given by

$$u(\mathbf{r}) = \sum_{n=l}^\infty a_n u_{mn}(\mathbf{r}), \quad (5)$$

where only basis functions with the same azimuthal index m have to be taken into account and $a_n = 0$ if $n < l$. The expansion coefficients in the source-free region are determined via the addition theorem for scalar multipoles [53,54]. Here, the expansion coefficients are

$$a_n = U_0(-1)^m\sqrt{\frac{(2m)!(n - m)}{(n + m)!}}\sum_p(-1)^p g_p(kz_0 \mathrm{i})(2p + 1)$$

$$\times \begin{pmatrix} m & n & p \\ m & -m & 0 \end{pmatrix}\begin{pmatrix} m & n & p \\ 0 & 0 & 0 \end{pmatrix}, \quad (6)$$

where Wigner-$3j$ symbols appear twice in the sums and $n + m \geqslant p \geqslant |n - m|$ (see [53,54]). Unfortunately, calculation of the expansion coefficients using Eq. (6) involves a summation that depends on the increasing number of terms n, therefore, it is unpractical. We were unable to find in the literature an addition theorem for spherical Bessel functions for orders higher

than zero, therefore, we have developed it for our particular displacement. We will now briefly discuss steps leading to it.

We note that the second Wigner $3j$ requires $m + n + p$ to be an even number, therefore, index p changes by multiples of two. On the other hand, we note that $g_\nu(x)/x^\mu$ can be expressed as a similarly behaving sum via the following recursion:

$$\frac{g_\nu(x)}{x^\mu} = \frac{1}{2\nu + 1} \frac{g_{\nu+1}(x) + g_{\nu-1}(x)}{x^{\mu-1}},$$

$$\frac{g_\nu(x)}{x^\mu} = \frac{(2\nu - 1)g_{\nu+2} + 2(2\nu + 1)g_\nu + (2\nu + 3)g_{\nu-2}}{(2\nu - 1)(2\nu + 1)(2\nu + 3)x^{\mu-2}},$$

$$\cdots$$

$$\frac{g_\nu(x)}{x^\mu} = \sum_{\nu+\mu \geqslant p \geqslant |\nu-\mu|} b_p g_p(x), \tag{7}$$

and the sum $\nu + \mu + p$ is always an even number as in Eq. (6). Unfortunately, the derivation is too lengthy to print, so for the sake of brevity we omit it here. We have identified the coefficients b_p as a combination of gamma functions and compared them with those from (6). It turns out that expansion coefficients a_n can be readily expressed as

$$a_n = U_0(2n + 1)(2l - 1)!! \frac{g_n(ikz_0)}{(ikz_0)^l}, \quad m \geqslant 0$$

$$a_n = U_0(2n + 1) \frac{1}{2^l l!} \frac{(n + l)!}{(n - l)!} \frac{g_n(ikz_0)}{(ikz_0)^l}, \quad m \leqslant 0 \tag{8}$$

where double factorial $(2l - 1)!! = 2^{-l}(2l)!/l!$ was introduced and $-1!! = 1$. To obtain the irregular (regular) solution we replace function g_p by h_p (j_p). For the rest of the paper we mainly consider the regular solution $u(\mathbf{r})$. The irregular solution will be briefly discussed where necessary. The first $(n = l)$ expansion coefficient is always a constant number $a_l = (2l + 1)!!$ due to the normalization constant U_0 [see Eq. (3)].

B. Expansion of vectorial vortex beams within spherical symmetry

From the scalar solution $u(\mathbf{r})$ we construct dimensionless azimuthally $\mathbf{U}_M^{(s)}$ and radially $\mathbf{U}_N^{(s)}$ polarized vector complex source beams as in [16,19]

$$\mathbf{U}_M^{(s)}(\mathbf{r}) = \nabla u(\mathbf{r}) \times \mathbf{r}, \quad \mathbf{U}_N^{(s)}(\mathbf{r}) = \frac{1}{k} \nabla \times \mathbf{U}_M(\mathbf{r}). \tag{9}$$

They represent the electric and magnetic fields of a vector beam with spherical symmetry (see [19]). The so-called "vortex cores" [19] of $\mathbf{U}_M^{(s)}$ and $\mathbf{U}_N^{(s)}$ reveal a complex structure, which can be compactly expressed in cylindrical coordinates (ρ, ϕ, z) as

$$\mathbf{U}_M^{(s)} = U_0 \rho^{m-1} e^{i\alpha m\phi} e^{ikz}[\mathbf{e}_\rho z i\alpha m$$

$$- \mathbf{e}_\phi(mz - ik\rho^2\theta) - \mathbf{e}_z i\alpha m\rho],$$

$$\mathbf{U}_N^{(s)} = \frac{U_0}{k} \rho^{m-1} e^{i\alpha m\phi} e^{ikz}\{\mathbf{e}_\rho[m(m + 1) + ikzm + k^2\rho^2]$$

$$+ i\alpha m\mathbf{e}_\phi(m + 1 + ikz) + \mathbf{e}_z ik\rho(m + 2)\}. \tag{10}$$

Here, $\mathbf{e}_\rho, \mathbf{e}_\phi, \mathbf{e}_z$ are unitary direction vectors. We note that the beam $\mathbf{U}_N^{(s)}$ looks similar to the so-called "flower," discussed

in Ref. [55]. Experimental realization of these CSVs can be understood looking at the far-field structure, which has a compact representation in spherical coordinates ($\mathbf{e}_\theta$ and $\mathbf{e}_\phi$ are spherical unit vectors) [19]

$$\mathbf{U}_M^{(s)} = \sin^{m-1}\theta e^{i\alpha m\phi}[i\alpha m g_m \mathbf{e}_\theta - (m\cos\theta g_m$$

$$- ikz_0 \sin^2\theta g_{m+1})\mathbf{e}_\phi],$$

$$\mathbf{U}_N^{(s)} = \sin^{m-1}\theta e^{i\alpha m\phi}[(-m\cos\theta g_{m+1}$$

$$+ ikz_0 \sin^2\theta g_{m+2})\mathbf{e}_\theta - im\alpha g_{m+1}\mathbf{e}_\phi]. \tag{11}$$

The family of the orthogonal VSHs $\mathbf{M}_{\mu\nu}$, $\mathbf{N}_{\mu\nu}$, defined in Ref. [40] are obtained from the scalar spherical multipoles (4) after applying the same operators as in Eq. (9). Further, the substitution of the sum (5), which represents a scalar CSV, into Eq. (9) results in the following expansions of radially and azimuthally polarized vortex beams into VSHs, which we write as

$$\mathbf{U}_M^{(s)} = \sum_{n=l}^\infty A_n^{(s)} \widetilde{\mathbf{M}}_{mn}, \quad \mathbf{U}_N^{(s)} = \sum_{n=l}^\infty A_n^{(s)} \widetilde{\mathbf{N}}_{mn}, \tag{12}$$

where $\widetilde{\mathbf{M}}_{mn} = \gamma_{mn}\mathbf{M}_{mn}$ and $\widetilde{\mathbf{N}}_{mn} = \gamma_{mn}\mathbf{N}_{mn}$ are normalized VSHs, defined in Ref. [40]. The γ_{mn} are the standard normalization constants (see [40]), and the normalized expansion coefficients thus are $A_n^{(s)} = a_n/\gamma_{mn}$. For zero complex displacement $z_0 = 0$, Eqs. (9) reduce to the vector-spherical harmonics (VSH) $\mathbf{M}_{ml}$ and $\mathbf{N}_{ml}$ (see [56]). We note here that complexly displaced VSHs were studied by Moore *et al.* [49]. However, the spherical nabla and the displacement operators do not commute, therefore, Eqs. (9) represent a different family of beams. Indeed, a complex displacement of an electric (magnetic) multipole in the z direction will result in the expansion where not only electric (magnetic) but also magnetic (electric) multipoles will appear. In contrast to that, we observe in the expansion (12) that only electric (magnetic) multipoles are present.

The dependence of the expansion coefficients $A_n^{(s)}$ on the collimation distance kz_0 and the multipole order n is shown in Fig. 1. As it was pointed out, the very first expansion coefficient $A_l^{(s)}$ does not depend on kz_0 due to our definition of the normalization constant and the coefficient can be expressed as $A_l^{(s)} = (2l + 1)!!/\gamma_{ll}$. As the beam becomes unfocused, the maximal contribution is shifted from multipole with $n = l$ into a higher multipole. Here we note that the differences in the expansion coefficients between regular and irregular complex source beams appear only at values of the collimation distance $kz_0 < n$. The natural cause for this divergent behavior is the presence of virtual sources in the irregular beam [19].

C. Expansion of cylindrically symmetric vectorial complex source vortices

The dimensionless CSB vortices with cylindrical symmetry $\mathbf{U}_M^{(c)}$ and $\mathbf{U}_N^{(c)}$ are defined by [19]

$$\mathbf{U}_M^{(c)}(\mathbf{r}) = \nabla u(\mathbf{r}) \times \frac{\mathbf{e}_z}{k}, \quad \mathbf{U}_N^{(c)}(\mathbf{r}) = \frac{1}{k} \nabla \times \mathbf{U}_M^{(c)}(\mathbf{r}), \tag{13}$$

where $\mathbf{e}_z = \mathbf{e}_r \cos\theta - \mathbf{e}_\theta \sin\theta$, here $\mathbf{e}_r$ is a unit vector of the spherical coordinates. They represent the electric and magnetic fields of a vector vortex within cylindrical symmetry.
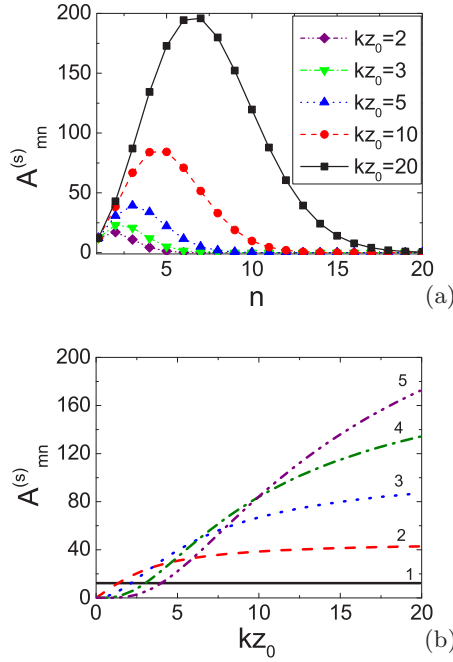
FIG. 1. (a) Dependence of the different expansion coefficients $|A_{mn}^{(s)}|$ on the multipole order for regular solutions for different kz_0. (b) Dependence of the different expansion coefficients $|A_{mn}^{(s)}|$ on the collimation distance kz_0 for regular and irregular solutions. The multipole order n is shown in the graph. The topological charge $m = 1$.

Solution $\mathbf{U}_M^{(c)}$ ($\mathbf{U}_N^{(c)}$) represents a transverse with respect to the vector $\mathbf{e}_z$ electric (magnetic) electromagnetic field. The "vortex cores" of $\mathbf{U}_M^{(c)}$ and $\mathbf{U}_N^{(c)}$ are given by

$$\mathbf{U}_M^{(c)} = U_0 i\alpha m \rho^{m-1} e^{i\alpha m \phi} e^{ikz}(\mathbf{e}_\rho + i\alpha \mathbf{e}_\phi),$$

$$\mathbf{U}_N^{(c)} = U_0 im \rho^{m-1} e^{i\alpha m \phi} e^{ikz}(\mathbf{e}_\rho + i\alpha \mathbf{e}_\phi). \quad (14)$$

Once again we see a rather complex structure: the beam $\mathbf{U}_M^{(c)}$ has a pattern similar to the flower and the beam $\mathbf{U}_N^{(c)}$ resembles a web (see Ref. [55]). Experimentally, such CSVs can be realized by creation of the following spatial spectra (far field) [19]:

$$\mathbf{U}_M^{(c)} = -kU_0 \sin^{m+1}\theta e^{i\alpha m\phi} g_{m+1}\mathbf{e}_\phi,$$

$$\mathbf{U}_N^{(c)} kU_0 \sin^{m+1}\theta e^{i\alpha m\phi} g_{m+2}\mathbf{e}_\theta. \quad (15)$$

Next, we need to decompose the vector function $k^{-1}\mathbf{L}_{mn} \times \mathbf{e}_z$, where $\mathbf{L}_{mn}$ is a nonsolenoidal VSH [12]. Next, we take advantage of the fact that the functions $\mathbf{N}_{mn}$ have a nonzero radial component at the origin $r \to 0$. The decomposition into $\mathbf{M}_{mn}$ is performed on the other hand at infinity $r \to \infty$. The complicated integration is omitted here and the final expression is given as

$$\mathbf{L}_{mn} \times \frac{\mathbf{e}_z}{k} = \frac{im}{n(n+1)}\mathbf{N}_{m,n} + \frac{n+m}{n(2n+1)}\mathbf{M}_{m,n-1}$$

$$+ \frac{n+1-m}{(n+1)(2n+1)}\mathbf{M}_{m,n+1}. \quad (16)$$

We note that an electric multipole $\mathbf{N}_{m,n}$ appears in the expression in order to ensure the transversality of the resulting

electric field in respect to the $\mathbf{e}_z$ (see [19] for a more detailed discussion on that).

The decomposition contains only terms with azimuthal index m, so the highly focused vortices are expressed by the sum

$$\mathbf{U}_M^{(c)} = \sum_{n=1}^{\infty} A_n^{(c)}\widetilde{\mathbf{M}}_{mn} + B_n^{(c)}\widetilde{\mathbf{N}}_{mn},$$

$$\mathbf{U}_N^{(c)} = \sum_{n=1}^{\infty} B_n^{(c)}\widetilde{\mathbf{M}}_{mn} + A_n^{(c)}\widetilde{\mathbf{N}}_{mn}, \quad (17)$$

where

$$\gamma_{mn}A_n^{(c)} = \left[\frac{a_{n+1}(n+m+1)}{(n+1)(2n+3)} + \frac{a_{n-1}(n-m)}{n(2n-1)}\right],$$

$$\gamma_{mn}B_n^{(c)} = \frac{ima_n}{n(n+1)}. \quad (18)$$

We note that the electric (magnetic) multipole disappears in the solution $\mathbf{U}_M^{(c)}$ ($\mathbf{U}_N^{(c)}$), if the topological charge m of the vortex is zero. Moreover, it can be demonstrated that the expansion coefficient $A_n^{(c)}$ becomes proportional to the expansion coefficient $A_n^{(s)}$ from the previous section (see [46]). This is a direct consequence of the fact that radially and azimuthally polarized beams with no topological charges can be derived within both spherical and cylindrical symmetry (see [16]).

The dependence of the multipole amplitudes $A_n^{(c)}$ and $B_n^{(c)}$ on the multipole order for different values of kz_0 is presented in Fig. 2. The dependence of the amplitudes of the first five multipole components $A_{mn}^{(c)}$ and $B_{mn}^{(c)}$ on the collimation distance kz_0 are depicted in Figs. 2(c) and 2(d). We note here that for $n > l$ expansion coefficient $A_{mn}^{(c)}$ may become zero [Figs. 2(b) and 2(d)] because coefficients a_{n+1} and a_{n-1} have different signs. Thus, for known l and n exists a complex displacement kz_0 for which the multipole with indices m and n is not present [Fig. 2(d)].

For $kz_0 > n$ the expansion coefficients of the irregular solution do not differ significantly from that of the regular solution and the multipole with highest amplitude is always $n \to \infty$ due to the presence of virtual sources in the irregular beam (see [15]). An example of intensity distributions for the cylindrically symmetric beams $\mathbf{U}_M^{(c)}$, $\mathbf{U}_N^{(c)}$ is available in Ref. [19].

D. Expansion of circularly polarized vortex beams

Dimensionless circularly polarized beams are defined as [19]

$$\mathbf{U}_M^{(\beta)}(\mathbf{r}) = \nabla u(\mathbf{r}) \times \frac{\mathbf{e}_\beta}{k}, \quad \mathbf{U}_N^{(\beta)}(\mathbf{r}) = \frac{1}{k}\nabla \times \mathbf{U}_M^{(\beta)}(\mathbf{r}), \quad (19)$$

where $\mathbf{e}_\beta = \mathbf{e}_x + i\beta\mathbf{e}_y$ here $\beta = \pm 1$ is the the handedness. Cartesian unit vectors are $\mathbf{e}_x$ and $\mathbf{e}_y$. Two pairs of left- and right-handed circularly polarized vector vortices are possible. The vortex cores of circularly polarized vortices are [19] given
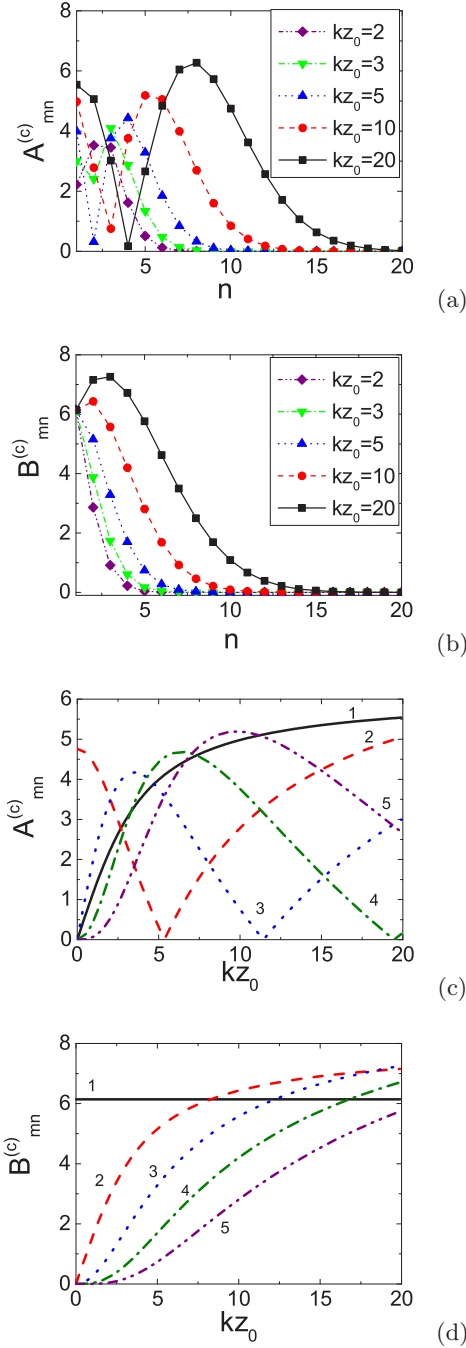
FIG. 2. Dependence of the different expansion coefficients $|A_{mn}^{(c)}|$ (a) and $|B_{mn}^{(c)}|$ (b) on the multipole order for regular solutions for different kz_0. Dependence of the different expansion coefficients $|A_{mn}^{(s)}|$ (c) and $|B_{mn}^{(c)}|$ (d) on the collimation distance kz_0 for regular and irregular solutions. The multipole order n is shown in the graph. The topological charge $m = 1$.

by

$$\mathbf{U}_M^{(\beta)} = U_0 e^{ikz}[\mathbf{e}_\beta \beta k(x + i\alpha y)^m + \mathbf{e}_z im(\beta - \alpha)(x + i\alpha y)^{m-1}],$$

$$\mathbf{U}_N^{(\beta)} = U_0 k^{-1} e^{ikz}[\mathbf{e}_\alpha m(m-1)(1 - \alpha\beta)(x + i\alpha y)^{m-2}$$
$$+ \mathbf{e}_\beta k^2(x + i\alpha y)^m + \mathbf{e}_z ikm(1 - \alpha\beta)(x + i\alpha y)^{m-1}]. \tag{20}$$

We note that the beam $\mathbf{U}_M^{(\beta)}$ looks similar to the so-called spider webs and flowers, discussed in Ref. [55]. In overall, the first circularly polarized vortex solution $\mathbf{U}_M^{(\beta)}$ contains, in the near field, two vortices in its core: one is circularly polarized of the charge l and the second one longitudinally polarized of the charge $l - \alpha$. The second vortex solution $\mathbf{U}_N^{(\beta)}$ contains two or three vortices depending on the signs of α and β. The far fields are given by [19]

$$\mathbf{U}_M^{(\beta)} = U_0 k \sin^m \theta e^{i(\alpha m + \beta)\phi}(\mathbf{e}_\theta i\beta - \mathbf{e}_\phi \cos\theta)g_{m+1},$$

$$\mathbf{U}_N^{(\beta)} = -U_0 k \sin^m \theta e^{i(\alpha m + \beta)\phi}(\mathbf{e}_\theta \cos\theta + \mathbf{e}_\phi i\beta)g_{m+2}. \tag{21}$$

First, we decompose $k^{-1}\mathbf{L}_{mn} \times \mathbf{e}_+$, where $\mathbf{L}_{mn}$ is a nonsolenoidal VSH [12]. The final expression is

$$\mathbf{L}_{mn} \times \frac{\mathbf{e}_+}{k} = \sum_{\nu=1}^{\infty} \frac{i\delta_{\nu,n}}{\nu(\nu+1)}\mathbf{N}_{m+1,\nu}$$
$$- \left[\frac{\delta_{\nu,n+1}}{\nu(2\nu-1)} - \frac{\delta_{\nu,n-1}}{(\nu+1)2\nu+3}\right]\mathbf{M}_{m+1,\nu}. \tag{22}$$

The decomposition contains only terms with $m + 1$, so the circularly polarized beam can be expressed by the sum

$$\mathbf{U}_M^{(+)} = \sum_{n=1}^{\infty} A_n^{(+)} \widetilde{\mathbf{M}}_{m+1,n} + B_n^{(+)} \widetilde{\mathbf{N}}_{m+1,n},$$

$$\mathbf{U}_N^{(+)} = \sum_{n=1}^{\infty} A_n^{(+)} \widetilde{\mathbf{N}}_{m+1,n} + B_n^{(+)} \widetilde{\mathbf{M}}_{m+1,n}, \tag{23}$$

where

$$\gamma_{m+1,n} A_n^{(+)} = \left[\frac{a_{n-1}}{n(2n-1)} - \frac{a_{n+1}}{(n+1)(2n+3)}\right],$$

$$\gamma_{m+1,n} B_n^{(+)} = \frac{ia_n}{n(n+1)}. \tag{24}$$

The beams $\mathbf{U}_M^{(+)}$ and $\mathbf{U}_N^{(+)}$ are represented at the origin $\mathbf{r} = 0$ by circularly polarized electric and magnetic multipoles, whose azimuthal orders are by one order higher than the topological charge under consideration. The typical intensity and field patterns for one particular case are presented in Ref. [19].

The second pair of the beams $\mathbf{U}_M^{(-)}$ and $\mathbf{U}_N^{(-)}$ is expanded in the same fashion. The decomposition of the function $\mathbf{L}_{mn} \times \mathbf{e}_-$ into VSHs can be written as

$$\mathbf{L}_{mn} \times \frac{\mathbf{e}_-}{k} = \sum_{\nu=1}^{\infty} \frac{i\delta_{\nu,n}(\nu+m)(\nu-m+1)}{\nu(\nu+1)}\mathbf{N}_{m-1,\nu}$$
$$- \frac{\delta_{\nu,n-1}(\nu+m)(\nu+m+1)}{(\nu+1)(2\nu+3)}\mathbf{M}_{m-1,\nu}$$
$$+ \frac{\delta_{\nu,n+1}(\nu-m)(\nu-m+1)}{\nu(2\nu-1)}\mathbf{M}_{m-1,\nu} \tag{25}$$

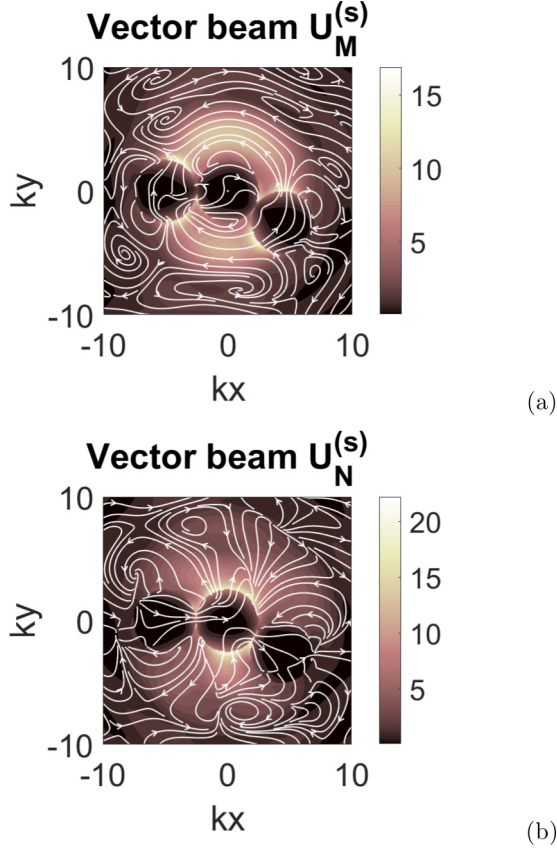**Vector beam U$_M^{(s)}$**

(a)

Vector beam U$_N^{(s)}$

(b)

FIG. 3. Modulus of the total field for transverse electric $\mathbf{U}_M^{(s)}$ (a) and transverse magnetic $\mathbf{U}_N^{(s)}$ (b) CSV scattered off the cluster of three gold spheres. The radii of spheres are $R_{sp} = 200$ nm, the wavelength is $\lambda = 500$ nm, the angle of the cluster is $\theta = 5\pi/6$ and $kz_0 = 5$. The white arrows depict the direction of the electric field $\mathbf{E}$.

Vector beam U$_M^{(s)}$ $\times 10^{-11}$

(a)

Vector beam U$_N^{(s)}$ $\times 10^{-11}$

(b)

FIG. 4. Modulus of the absolute error metric Λ between the total fields calculated using analytical expansion and finite-difference scheme for the cases of transverse electric $\mathbf{U}_M^{(s)}$ (a) and transverse magnetic $\mathbf{U}_N^{(s)}$ (b) CSV scattered off the cluster of three gold spheres. The radii of spheres are $R_{sp} = 200$ nm, the wavelength is $\lambda = 500$ nm, the angle of the cluster is $\theta = 5\pi/6$ and $kz_0 = 5$.

and the circularly polarized beams $\mathbf{U}_M^{(-)}$ and $\mathbf{U}_N^{(-)}$ are

$$\mathbf{U}_M^{(-)} = \sum_{n=1}^{\infty} A_n^{(-)}\widetilde{\mathbf{M}}_{m-1,n} + B_n^{(-)}\widetilde{\mathbf{N}}_{m-1,n},$$

$$\mathbf{U}_N^{(-)} = \sum_{n=1}^{\infty} A_n^{(-)}\widetilde{\mathbf{N}}_{m-1,n} + B_n^{(-)}\widetilde{\mathbf{M}}_{m-1,n}, \qquad (26)$$

where

$$\gamma_{m-1,n}A_n^{(-)} = \left[\frac{a_{n-1}(\nu-m)(\nu-m+1)}{n(2n-1)} \right.$$
$$\left. - \frac{a_{n+1}(\nu+m)(\nu+m+1)}{(n+1)(2n+3)} \right],$$

$$\gamma_{m-1,n}B_n^{(-)} = \frac{ia_n(\nu+m)(\nu-m+1)}{n(n+1)}. \qquad (27)$$

A variety of linear combinations can be constructed from the "pure" electric and magnetic linearly polarized beams: a tightly focused "mixed" circularly polarized vortex or a linearly polarized vortex [19]. The comparison of the first four expansion coefficients $A_n^{(\beta)}$, $B_{beta}^{(-)}$ reveals a a bell-shaped dependency on multipole order n. For the irregular solution expansion coefficients do not differ significantly as long as for
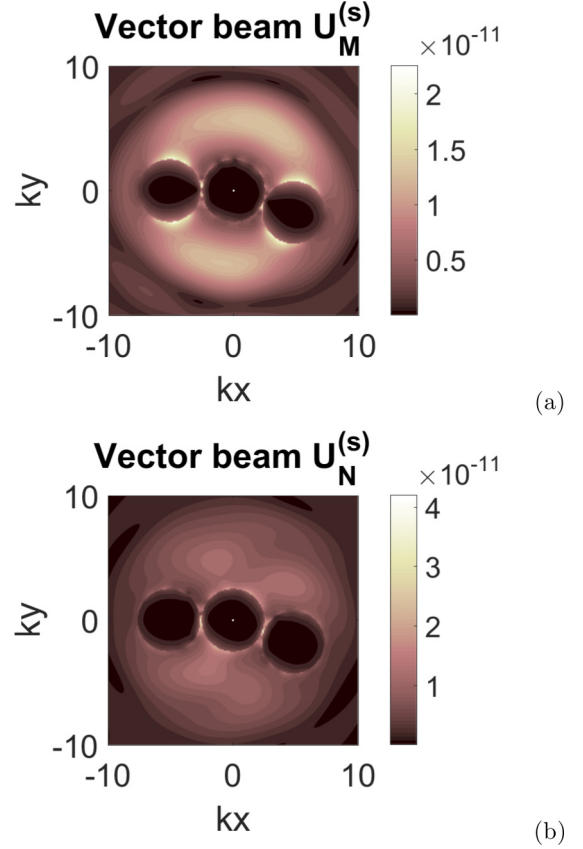
$kz_0 > n$, however, virtual sources cause an artificial increase in the expansion coefficients of very high multipoles.

III. APPLICATION TO MIE SCATTERING

In this section we use an analytical Mie-type theory for highly focused CSVs which interacts with a cluster of nanospheres situated in the origin. We start with a brief presentation of the basic idea of multiple scattering method (MSM) [57,58]. Suppose we have a cluster of N nonoverlapping spherical particles. We freely choose the global coordinates in which we denote the position of each particle as $\mathbf{r}^{(j)}$ and $\mathbf{r}^{(jl)}$, a vector pointing from particle with index j to the particle with index l. The scattered field $\mathbf{E}_{sca}^{(j)}(\mathbf{r}^{(j)})$ of each particle (j) can be written as

$$\mathbf{E}_s^{(j)}(\mathbf{r}^{(j)}) = \sum_{mn} P_{mn}^{(j)}\widetilde{\mathbf{M}}_{mn}^{(3)}(\mathbf{r}^{(j)}) + Q_{mn}^{(j)}\widetilde{\mathbf{N}}_{mn}^{(3)}(\mathbf{r}^{(j)}); \qquad (28)$$

this equation is valid for $r^{(j)} > R_{sp}$ and index (3) denotes irregular VSHs (see [40]). When coefficients $\mathbf{P}^{(j)}$, $\mathbf{Q}^{(j)}$ of the scattered field for particles with index j are known, then the

total electric field is given by

$$\mathbf{E}_{\text{tot}}(\mathbf{r}) = \mathbf{E}_i(\mathbf{r}) + \sum_j \mathbf{E}_s^{(j)}(\mathbf{r}^{(j)}). \qquad (29)$$

The light scattered by a nanoparticle can be expressed as a sum of the irregular VSHs and conveniently written as a vector $\mathbf{E}_s = \mathbf{T}\mathbf{E}_i$, where we introduce the concept of the T matrix [40], which relates the vector representations of scattered and incident fields. Coefficients $\mathbf{P}^{(j)}$, $\mathbf{Q}^{(j)}$ of the scattered field $\mathbf{E}_s^{(j)}$ are related to coefficients $\mathbf{A}^{(j)}$, $\mathbf{B}^{(j)}$ of the incident field $\mathbf{E}_i(\mathbf{r})$ by T matrix as $(\mathbf{P}^{(j)}, \mathbf{Q}^{(j)})^T = \mathbf{T}^{(j)}(\mathbf{A}^{(j)}, \mathbf{B}^{(j)})^T$. Here $\mathbf{T}^{(j)}$ is a transfer matrix of an individual particle with index j and $(\mathbf{A}^{(j)}, \mathbf{B}^{(j)})$ are expansion coefficients of the incident field $\mathbf{E}_i(\mathbf{r})$ in the local coordinate frame of the particle with index j. In this formalism the electric field incident on a particle with index j is a superposition of the incoming beam $\mathbf{E}_i$ and the scattered field from other particles $\mathbf{E}_s^{(l)}$:

$$\mathbf{E}_i^{(j)}(\mathbf{r}) = \mathbf{E}_{\text{inc}}(\mathbf{r}) + \sum_{l \neq j} \mathbf{E}_s^{(l)}(\mathbf{r}). \qquad (30)$$

This leads us to the following equation for the unknowns $\mathbf{P}^{(j)}$, $\mathbf{Q}^{(j)}$:

$$\begin{pmatrix} \mathbf{P}^{(j)} \\ \mathbf{Q}^{(j)} \end{pmatrix} = \mathbf{T}^{(j)} \left[\mathbf{D}_{(j,O)}^{(1)} \begin{pmatrix} \mathbf{A} \\ \mathbf{B} \end{pmatrix} + \sum_{l \neq j} \mathbf{D}_{(j,l)}^{(2)} \begin{pmatrix} \mathbf{P}^{(j)} \\ \mathbf{Q}^{(j)} \end{pmatrix} \right]. \qquad (31)$$

Here, $\mathbf{D}_{(j,l)}^{(1)}$, $\mathbf{D}_{(j,l)}^{(2)}$ denote first and second kind displacement operators for VSH coefficients, respectively (see more on definition in Refs. [8,57–59]). $(\mathbf{A}, \mathbf{B})$ are expansion coefficients of the incident field $\mathbf{E}_i(\mathbf{r})$ in the coordinate frame of the beam. After determining unknowns from (31) we can determine not only electric and magnetic fields outside and inside particles but calculate such parameters as transmission, reflection also, with the use of the methodology described in the Appendices of Refs. [8,59].

We build a trimer nanocluster from homogeneous gold spheres with a radius $R_{sp} = 200$ nm and a complex refractive index $n_{sp} = 0.9726 + 1.8501i$ [60] embedded in a homogeneous nonabsorbing medium with refractive index $n_m = 1$ at the wavelength of 500 nm. We arrange particles in the cluster so that the angle θ between two arms is $\theta = 5\pi/6$ and the particles have a small gap of 10 nm between them.

We have chosen these parameters to ensure a rich multipolar response of the nanocluster [37,42] and to showcase different interactions with various vector complex sourced vortices. On the other hand, our wish is to avoid strong resonances, as they might require high numbers of multipoles for the code to converge (see Refs. [61,62]). Another motivation behind our choice were recent presentations of chirality in planar cluster structures [41,42,63]. So, the cluster under investigation is slightly chiral [42]. We have used the value of the complex displacement $kz_0 = 5$ for all the beams in the study; they also had the same initial topological charge $m = 1$. We have used in our calculations up to 20 expansion coefficients. It was more than enough for this case.

First, we examine the distribution of a total electric field when the cluster was placed in the center of the spherically symmetric beams $\mathbf{U}_M^{(s)}$, $\mathbf{U}_N^{(s)}$. We plot the modulus of the dimensionless total electric field in the transverse plane [see Figs. 3(a) and 3(b)]. The transverse electric solution $\mathbf{U}_M^{(s)}$ has no radial components of the electric field; it contains magnetic multipoles and two (first one and third one) particles in the cluster are excited efficiently. One might note excitation of the electric dipoles' multipoles on the surface of two marginally excited particles, while none on the central unexcited particle. The second beam $\mathbf{U}_N^{(s)}$ contains electric multipoles and the central particle in the cluster interacts with the field more strongly than other two [see Fig. 3(b)].

In order to prove a validity and test accuracy of the MSM implementation, we have implemented a finite-difference scheme (based on FDTD++, see Ref. [64]), which calculates Mie-type scattering of CSVs from multiple spheres. First, we have tested the developed tool with known theoretical solutions and other available tools from Ref. [65] and have found no meaningful differences. Additionally, we had tested it under the same conditions using a commercial software from Ansys/Lumerical [42]. We have considered two error metrics: an absolute and a relative one. Unfortunately, as the electric field approaches near zero values, values of the relative error approach infinity. For this reason we consider here the dimensionless absolute error metric Λ to evaluate the difference between the results retrieved from MSM implementation and numerical tool:

$$\Lambda = \sqrt{\left(\left| E_x^{(1)} \right| - \left| E_x^{(2)} \right| \right)^2 + \left(\left| E_y^{(1)} \right| - \left| E_y^{(2)} \right| \right)^2 + \left(\left| E_z^{(1)} \right| - \left| E_z^{(2)} \right| \right)^2}, \qquad (32)$$

where $\mathbf{E}^{(1)} = (E_x^{(1)}, E_y^{(1)}, E_z^{(1)})$ is the electric field calculated using analytical expansion together with MSM method and $\mathbf{E}^{(2)} = (E_x^{(2)}, E_y^{(2)}, E_z^{(2)})$ is the electric field obtained using the finite-difference scheme. The resulting error measure is plotted in Figs. 4(a) and 4(b). We note that a slight difference is present (it has an order of 10^{-11}). The main cause for the difference to appear is the number of multipoles used in expansions of fields ($N = 20$). The increase of the multipoles drastically reduces the error measure in the expense of longer computation times. Obviously, there are two causes

of introduction of the errors: first is the expansion of the incident beam into multipoles using VSH's, larger number of multipoles reduces the difference between the exact beam distribution and the decomposed one. Second is the way of scattered field description in Eq. (31), the response of the cluster has much richer multipolar response than a single particle. In the FDTD schemes, errors can occur due to many causes coming from grid selection, boundary conditions, calculation methods, etc.; here, the largest value of Λ at the interparticle region, because it is the most sensitive, is due to the local field enhancements [61,62]. Overall, the presented implementation
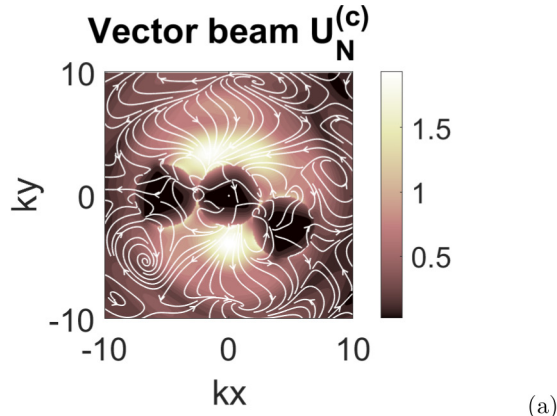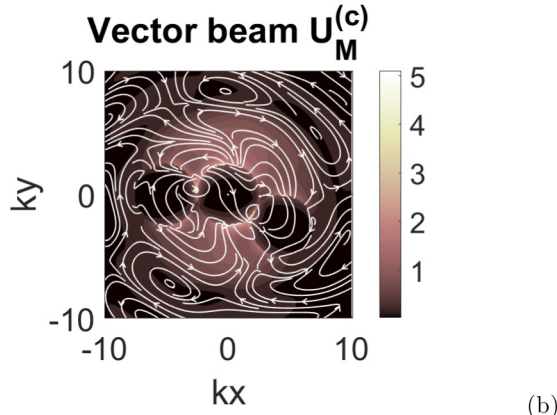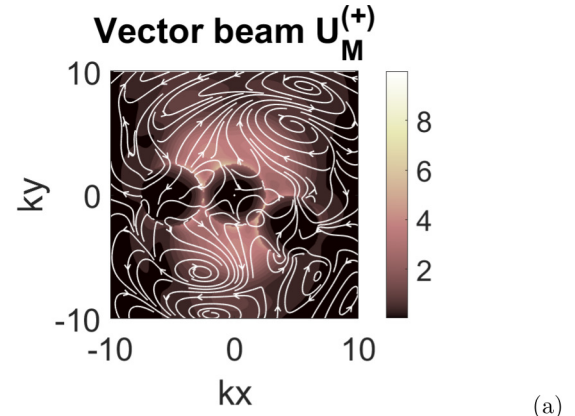
FIG. 5. Modulus of the total field for transverse electric $\mathbf{U}_M^{(c)}$ (a) and transverse magnetic $\mathbf{U}_N^{(c)}$ (b) CSV scattered off the cluster of three gold spheres. The radii of spheres are $R_{sp} = 200$ nm, the wavelength is $\lambda = 500$ nm, the angle of the cluster is $\theta = 5\pi/6$ and $kz_0 = 5$. The white arrows depict the direction of the electric field $\mathbf{E}$.

FIG. 6. Modulus of the total field for transverse electric $\mathbf{U}_M^{(\beta)}$ CSB scattered off the cluster of three gold spheres. The radii of spheres are $R_{sp} = 200$ nm, the wavelength is $\lambda = 500$ nm, the angle of the cluster is $\theta = 5\pi/6$ and $kz_0 = 5$, the handedness is $\beta = 1$ (a) and $\beta = -1$ (b). The white arrows depict the direction of the electric field $\mathbf{E}$.
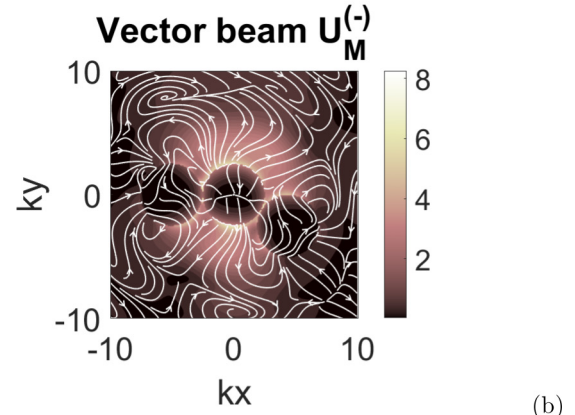
has successfully converged and describes the physical situation on the acceptable level of accuracy.

We have also investigated electric field distribution when the same trimer cluster is placed in the center of cylindrically symmetric beams $\mathbf{U}_M^{(c)}$, $\mathbf{U}_N^{(c)}$ [see Figs. 5(a) and 5(b)]. The transverse electric solution $\mathbf{U}_M^{(c)}$ has no z components of the electric field [19]; this automatically leads to an appearance of a electric dipole [see Eq. (17)] and therefore the central particle is also excited. The central particle of the cluster placed in the the beam $\mathbf{U}_N^{(c)}$ is excited mostly [see Fig. 5(b)]. As the result of scattering the transversality of the electric field is perturbed. Due to the presence of the longitudinally polarized magnetic dipole, particles adjacent to the central one are also slightly excited.

Lastly, circularly polarized complex source vortices are investigated. We consider two different handednesses for magnetic-type modes $\mathbf{U}_M^{(\beta)}$ [see Figs. 6(a) and 6(b)]. These modes represent tightly focused circularly polarized vortices, which were already studied in a similar situation elsewhere (see Refs. [41,42,63]). A comparison with other beams reveals that the cluster is excited stronger than in the previous case. The incident field is barely seen in the background. This cluster is slightly chiral, so one can observe slightly higher

response to the vortex $\mathbf{U}_M^{(+)}$ than to the beam with negative handedness $\beta = -1$.

IV. CONCLUSION

In conclusion, we have exploited the regular and irregular scalar CSV model to develop an analytical expansion of variously polarized vector CSVs into VSHs. We have presented closed-form compact analytical expansion of vector vortices within spherical, cylindrical, and Cartesian symmetries. The differences between regular and irregular vector beams diminish, when beam waist and collimation distance remains large. However, when the beam waist reaches the size of the collimation distance, higher-order multipoles dominate in the expansion of irregular highly focused complex source beams carrying vortices, therefore, the model does not describe anymore the physical situation properly.

Different types of complexifed vector vortices are described by electromagnetic multipoles having various indices m, n. The spherically symmetric vector vortices have only either magnetic ($\mathbf{U}_M^{(s)}$) or electric ($\mathbf{U}_N^{(s)}$) multipoles in their expansions. The cylindrically symmetric vector vortices contain both electric and magnetic type multipoles. Changes in the collimation distance nontrivially influence expansion co-

efficients $A^{(c)}$ and it might even vanish. In both symmetries, the topological charge of the vortex m coincides with the azimuthal index of the VSH. For circularly polarized vortices, the topological charge enters azimuthal dependency as $m + \beta$, so the multipolar structure is different because of the presence of the spin angular momentum. This situation is known as the conversion of the spin angular momentum into orbital.

The Mie scattering of the vector complex source vortices on a small golden trimer was investigated in detail. We report on differences in the multipolar excitation of the nanotrimer under investigation for three different types of vector complex source beams, namely, spherically symmetric, cylindrically symmetric, and circularly polarized. We demonstrate that magnetic and electric type beams excite different individual nanoparticles in the cluster. In our opinion, a different multipolar structure of vectorial CSVs enables a selective excitation of rather high-order Mie multipoles [36,37] and therefore is essential for studies of such properties as birefringence [42] and chirality [41,63] in clustered structures.

[1] G. Mie, Ann. Phys. **25**, 377 (1908).

[2] S. Quabis, R. Dorn, M. Eberler, O. Glöckl, and G. Leuchs, Opt. Commun. **179**, 1 (2000).

[3] R. Dorn, S. Quabis, and G. Leuchs, Phys. Rev. Lett. **91**, 233901 (2003).

[4] P. Banzer, U. Peschel, S. Quabis, and G. Leuchs, Opt. Express **18**, 10905 (2010).

[5] P. Banzer, J. Kindler, S. Quabis, U. Peschel, and G. Leuchs, Opt. Express **18**, 10896 (2010).

[6] T. Bauer, S. Orlov, G. Leuchs, and P. Banzer, Appl. Phys. Lett. **106**, 091108 (2015)

[7] A. Bag, M. Neugebauer, P. Wozniak, G. Leuchs, and P. Banzer, Phys. Rev. Lett. **121**, 193902 (2018)

[8] T. Bauer, S. Orlov, U. Peschel, P. Banzer, and G. Leuchs, Nat. Photonics **8**, 23 (2014).

[9] T. Bauer, P. Banzer, E. Karimi, S. Orlov, A. Rubano, L. Marrucci, E. Santamato, R. W. Boyd, and G. Leuchs, Science **347**, 964 (2015)

[10] T. Bauer, P. Banzer, F. Bouchard, S. Orlov, L. Marrucci, E. Santamato, R. W. Boyd, E. Karimi, and G. Leuchs, New J. Phys. **21**, 053020 (2019)

[11] A. E. Siegman, *Lasers* (University Science Books, Sausalito, CA, 1986).

[12] J. Stratton, *Electromagnetic Theory* (McGraw-Hill, New York, 1940).

[13] A. Wunsche, J. Opt. Soc. Am. A **5**, 765 (1992).

[14] A. M. Tagirdzhanov and A. M. Kiselev, Opt. Spectrosc. **119**, 257 (2015).

[15] C. J. R. Sheppard and S. Saghafi, J. Opt. Soc. Am. A **16**, 1381 (1999).

[16] S. Orlov and U. Peschel, Phys. Rev. A **82**, 063820 (2010).

[17] F. G. Mitri, Phys. Rev. E **89**, 023205 (2014).

[18] F. G. Mitri, Phys. Rev. A **94**, 023801 (2016).

[19] S. Orlov and P. Banzer, Phys. Rev. A **90**, 023832 (2014).

[20] B. Richards and E. Wolf, Proc. R. Soc. A: Math. Phys. Eng. Sci. **253**, 358 (1959).

[21] J. F. Nye and M. V. Berry, Proc. R. Soc. A: Math. Phys. Eng. Sci. **336**, 165 (1974).

[22] I. Freund and N. Shvartsman, Phys. Rev. A **50**, 5164 (1994).

[23] G. A. Turnbull, D. A. Roberson, G. M. Smith, L. Allen, and M. J. Padgett, Opt. Commun. **127**, 183 (1996).

[24] M. W. Beijersbergen, L. Allen, H. van der Veen, and J. P. Woerdman, Opt. Commun. **96**, 123 (1993).

[25] V. Yu. Bazhenov, M. V. Vasnetsov, and M. S. Soskin, Pis'ma Zh. Eksp. Teor. Fiz. **52**, 1037 (1990) [JETP Lett. **52**, 429 (1990)].

[26] V. Jarutis, R. Paskauskas, and A. Stabinis, Opt. Commun. **184**, 105 (2000).

[27] H. He, N. R. Heckenberg, and H. Rubinsztein-Dunlop, J. Mod. Opt. **42**, 217 (1995).

[28] M. E. J. Friese, J. Enger, H. Rubinsztein-Dunlop, and N. R. Heckenberg, Phys. Rev. A **54**, 1593 (1996).

[29] M. Friese, T. Nieminen, N. R. Heckenberg, and H. Rubinsztein-Dunlop, Nature (London) **394**, 348 (1998).

[30] M. K. Kreysing, T. Kießling, A. Fritsch, C. Dietrich, J. R. Guck, and J. A. Käs, Opt. Express **16**, 16984 (2008).

[31] F. Hoerner, M. Woerdemann, S. Mueller, B. Maier, and C. Denz, J. Biophoton. **3**, 468 (2010).

[32] I. V. Basistiy, V. Yu. Bazhenov, M. S. Soskin, M. V. Vasnetsov, Opt. Commun. **103**, 422 (1993).

[33] S. Orlov, K. Regelskis, V. Smilgevičius, A. Stabinis, Opt. Commun. **209**, 155 (2002).

[34] S. Orlov, K. Regelskis, V. Smilgevicius, and A. Stabinis, J. Opt. A: Pure Appl. Opt. **6**, S255 (2004).

[35] V. A. Markel, V. N. Pustovit, S. V. Karpov, A. V. Obuschenko, V. S. Gerasimov, and I. L. Isaev, Phys. Rev. B **70**, 054202 (2004).

[36] P. Wozniak, P. Banzer, and G. Leuchs, Laser Photonics Rev. **9**, 231 (2015).

[37] T. Das, P. P. Iyer, R. A. DeCrescent, and J. A. Schuller, Phys. Rev. B **92**, 241110(R) (2015)

[38] T. X. Hoang, X. Chen, and C J. R. Sheppard, J. Opt. Soc. Am. A **29**, 32 (2012).

[39] X. Zambrana-Puyalto, X. Vidal, P. Wozniak, P. Banzer, and G. Molina-Terriza, ACS Photonics **5**, 2936 (2018)

[40] L. Tsang, J. A. Kong, and K.-H. Ding, *Scattering of Electromagnetic Waves* (Wiley, New York, 2000).

[41] P. Banzer, P. Wozniak, U. Mick, I. De Leon, and R. W. Boyd, Nat. Commun. **7**, 13117 (2016)

[42] K. Laurinavičius, J. Berškys, and S. Orlov, *Photonic and Phononic Properties of Engineered Nanostructures X*, Vol.

11289 (SPIE: International Society for Optics and Photonics, Bellingham, WA, 2020), p. 112891Z.

[43] C. J. R. Sheppard and S. Saghafi, Phys. Rev. A **57**, 2971 (1998).

[44] N. J. Moore and M. A. Alonso, Opt. Express **16**, 5926 (2008).

[45] N. J. Moore and M. A. Alonso, J. Opt. Soc. Am. A **26**, 1754 (2009).

[46] X. Y. Zhang, Y. Q. Guo, P. Pei, and X. X. Yi, Phys. Rev. A **95**, 063825 (2017).

[47] A. K. Singh, S. Saha, S. D. Gupta, and N. Ghosh, Phys. Rev. A **97**, 043823 (2018)

[48] S. A. R. Horsley, C. G. King, and T. G. Philbin, J. Opt. **18**, 044016 (2016).

[49] N. J. Moore and M. A. Alonso, J. Opt. Soc. Am. A **26**, 2211 (2009).

[50] R. Gutierrez-Cuevas, N. J. Moore, and M. A. Alonso, Phys. Rev. A **97**, 053848 (2018).

[51] T. X. Hoang, S. N. Nagelberg, M. Kolle, and G. Barbastathis, Opt. Express **25**, 13125 (2017).

[52] S. N. Khonina and I. Golub, J. Opt. Soc. Am. B **36**, 2087 (2019).

[53] S. Stein, Q. Appl. Math. **19**, 1961 (1961).

[54] O. R. Cruzan, Q. Appl. Math. **20**, 33 (1962).

[55] E. Otte, K. Tekce, and C. Denz, Opt. Express **25**, 20194 (2017).

[56] P. M. Morse and H. Feshbach, *Methods of Theoretical Physics*, Volume II (McGraw-Hill, New York, 1953).

[57] M. I. Mishchenko, L. D. Travis, and D. W. Mackowski, J. Quantum Spectrosc. Radiat. Transfer **55**, 535 (1996)

[58] D. W. Mackowski and M. I. Mishchenko, J. Opt. Soc. Am. A **13**, 2266 (1996).

[59] M. Neugebauer, P. Banzer, T. Bauer, S. Orlov, N. Lindlein, A. Aiello, and G. Leuchs, Phys. Rev. A **89**, 013840 (2014).

[60] M. J. Weber, *Handbook of Optical Materials* (CRC Press, Boca Raton. FL, 2003).

[61] R. L. Chern, X. X. Liu, and C. C. Chang, Phys. Rev. E **76**, 016609 (2007).

[62] K. Sasihithlu and A. Narayanaswamy, Opt. Express **19**, A772 (2011).

[63] S. Orlov, J. Berškys, and K. Laurinavičius, *Complex Light and Optical Forces XIV*, Vol. 11297 (SPIE: International Society for Optics and Photonics, Bellingham, WA, 2020), p. 1129705.

[64] Finite-difference time domain (FDTD) software in C++, http://www.fdtdxx.com/.

[65] Light scattering software https://scattport.org/.